Applied Catalysis B: Environmental 198 (2016) 480–492

Contents lists available at ScienceDirect

Applied Catalysis B: Environmental

journal homepage: www.elsevier.com/locate/apcatb

Catalytic co-aromatization of ethanol and methane

Aiguo Wang[a], Peng He[a], Matthew Yung[b], Hongbo Zeng[c], Hui Qian[d], Hua Song[a,*]

[a] Department of Chemical and Petroleum Engineering, University of Calgary, 2500 University Drive, NW, Calgary, Alberta T2N 1N4, Canada
[b] National Bioenergy Center, National Renewable Energy Laboratory 15013 Denver West Parkway, Golden, CO 80401, United States
[c] Department of Chemical and Materials Engineering, University of Alberta 9211-116 Street NW, Edmonton, Alberta T6G 1H9, Canada
[d] National Institute for Nanotechnology, National Research Council, Edmonton, Alberta, T6G 2M9, Canada

ARTICLE INFO

Article history:
Received 4 February 2016
Received in revised form 18 May 2016
Accepted 3 June 2016
Available online 6 June 2016

Keywords:
Methane
Ethanol
Catalyst
Aromatization
ZSM-5

ABSTRACT

This study demonstrates the technical feasibility of simultaneously converting ethanol and methane into liquid hydrocarbons at mild reaction conditions (400 °C and 1 atm) over silver and/or zinc modified zeolite catalysts. After GC–MS analysis, it is worth noting that aromatics are the major compounds contained in the liquid product collected from the run when 1%Ag/ZSM-5, particularly after H_2 pretreatment, is charged. Compared to the performance exhibited from the run with pure HZSM-5 support engaged, Ag addition into the HZSM-5 framework favors aromatics formation, which might be closely associated with better Ag dispersion and more abundance of strong surface acidic sites where aromatization might take place while Zn loading exerts a detrimental effect on the production of aromatics but promotes the ether generation possibly through dehydration reaction. Referred to that from its N_2 counterpart, the increased aromatics formation of the collected liquid product when methane is present indicates that methane existence might facilitate ethanol aromatization. Moreover, combined with the increased carbon number in the formed aromatics from CH_4 run when H_2 run is referred and zero liquid formation from CH_4-alone test as well as more prominent endothermic feature of methane run and more importantly the notably increased ^{13}C signals in ^{13}C NMR spectra of the liquid product collected during ethanol conversion under $^{13}CH_4$ environment, all the observations suggest that methane might be activated nonoxidatively and converted into higher hydrocarbons, preferentially into aromatics if suitable catalyst is charged under the assistance of co-existing oxygenated hydrocarbon. The reported synergetic effect could potentially lead to the more economic utilization of abundant natural gas and cellulosic ethanol.

1. Introduction

Along with the economic growth and population increase, world energy demand has been increasing dramatically, especially over the last five decades (raised by 3.5 times since 1965 [1]). More importantly, more than 85% of the energy consumption still heavily relies on fossil fuels [2], the use of which poses many concerns including unsustainability and environmental pollution. Therefore, it is important to search for an energy carrier which is renewable and environmentally benign. Ethanol obtained from the fermentation of biomass seems desirable to serve as a green alternative due to its low toxicity, its ease of handling and its availability from many different renewable sources, ranging from cellulose to algae [3]. However, compared to its fossil fuel counterparts, the relative low volumetric energy density and high cost of ethanol still limit its wide implementation, thus leading to a strong need for its valorization.

Natural gas, including its recently largely discovered form (shale gas), is an abundant natural resource with ever increasing proved reserves (raised by more than 57% over the past 10 years) [1] and claimed as the cleanest energy carrier among fossil fuels because of its least particle matters generation and CO_2 emission (45% less than coal and 30% less than oil) when combusted. However, due to its chemical inertness and low volumetric energy density, natural gas is currently dominantly used for heating residential area and not valuable for transportation or chemical production applications. Therefore, natural gas is sold at much lower price ($0.23/GGE: gasoline gallon equivalent) than gasoline (~$2/GGE) even under the current ugly-looking oil economics. Intensive studies have been carried out over the past sixty years by many researchers regarding natural gas utilization and breakthrough has not yet been reported. Under such background, developing a technology which can effectively convert natural gas into valuable chemicals will definitely attract the attentions from both industry and academia.

* Corresponding author.
E-mail address: sonh@ucalgary.ca (H. Song).

http://dx.doi.org/10.1016/j.apcatb.2016.06.013
0926-3373/

Ethanol conversion into higher hydrocarbons has been intensively studied by many researchers over the past several decades [4–6] as an emerging alternative for ethanol valorization in addition to hydrogen production through steam reforming [7–9], among which aromatics formation through ethanol aromatization has been widely investigated with high popularity over zeolite supported catalyst due to its importance in chemical industries [10–12]. On the other hand, the conversion of methane, the main component of natural gas, into high value added chemicals has also drawn more and more attentions, particularly in recent years due to the vast exploitation of shale gas [13–15].

The state-of-art progresses in various directions for methane activation and utilization have been thoroughly reviewed by Tang, et al. [16] and Horn, et al. [17], among which methane dehydroaromatization deserves the most research concentration. In addition to the reforming of methane in an oxidative way for hydrogen production which has been well established in industry, aromatics formation from methane following a nonoxidative route has the most commercial potential because the reactant's energy is well remained into the liquid product with an additional benefit of generating valuable hydrogen as byproduct. Nonetheless, the requirement of extreme reaction conditions (e.g., high reaction temperature of at least 700 °C) and more importantly severe coke formation resulting in fast catalyst deactivation has to be managed in an appropriate and economical way before this process receives enough industrial attentions, which is mainly because of the high energy barrier for methane activation (~440 kJ/mol required for breaking down the first C—H bond in methane molecule) and poor selectivity toward aromatics from a thermodynamic viewpoint [18].

Nevertheless, thanks should be given to the promising work pioneered by Choudhary, et al. [19] and evidenced by a series of following publications [20–23] which indicates that methane conversion will be significantly improved in the presence of higher hydrocarbon and even oxygenated hydrocarbon reactants, particularly unsaturated hydrocarbons at much lower temperature region (400–600 °C) and atmospheric pressure, leading to the formation of liquid product abundant in aromatics. Among the synergetic effects reported, it is worth noting that Choudhary, et al. studied the simultaneous conversion of methanol and methane for the liquid hydrocarbons formation, which sets the background of this work [23]. In this paper, compared to that of its N_2 counterpart, higher amount of $C_{\geq 10}$ aromatics is obviously observed when methane is present over Mo-Zn/ZSM-5 at 500 °C and 1 atm, which might be due to the methane participation into the methanol aromatization reaction and further evidenced by engaging ^{13}C isotopic labeling technique. Moreover, the promotion effect of methane on ethanol aromatization is also briefly mentioned in the same paper but over Ga/ZSM-5 at temperature as high as 625 °C, which drives the motivation of seeking a new catalyst system for triggering the same reaction but at much lower temperature.

According to thermodynamic calculations, as expected methane aromatization is highly unfavorable, especially at lower temperatures. For instance, the reaction $6CH_4\,(g) = C_6H_6\,(g) + 9H_2\,(g)$ has Gibbs free energy ($\Delta_r G$) as high as 68.9 kcal/mol at 400 °C and 1 atm. Nevertheless, when ethanol is added as a co-reactant, $\Delta_r G$ of $2C_2H_6O\,(g) + 2CH_4\,(g) = C_6H_6\,(g) + 2H_2O\,(g) + 5H_2\,(g)$ is reduced significantly to −9.9 kcal/mol at the same reaction conditions, strongly suggesting the synergetic effect occurring between methane and ethanol and thermodynamic feasibility of their co-aromatization.

In this study, the technical feasibility of co-aromatization of ethanol and methane under mild conditions (400 °C and 1 atm) is experimentally demonstrated on Ag- and Zn-modified ZSM-5 zeolites. These catalysts were selected because they are reported to show promising performances toward biomass upgrading [24–26] and heavy oil upgrading [27] under methane environment in our previous studies. Significantly more aromatics formation was witnessed when 1%Ag/ZSM-5 was charged. This novel process will not only valorize ethanol produced from biomass fermentation and thus open a big market for its wider application, but also pave a more efficient, economical, and environmentally friendly way for methane utilization.

2. Experimental

2.1. Catalyst preparation

The ammonium ZSM-5 zeolite with Si/Al = 23 and specific surface area of 425 $m^2\,g^{-1}$ was purchased from Alfa Aesar and calcined at 600 °C for 5 h in air to attain the H-type ZSM-5 for further use. The 5%Zn-1%Ag/ZSM-5 was prepared by incipient wetness impregnation of H-ZSM-5 with $Zn(NO_3)_2{\cdot}6H_2O$ (99%, Alfa Aesar) and $AgNO_3$ (99.9+%, Alfa Aesar) solution, dried in the oven at 92 °C overnight, followed by being calcined at 600 °C for 3 h in ambient air. In a similar manner, 5%Zn/ZSM-5 and 1%Ag/ZSM-5 were also prepared for the experiments.

2.2. Sample characterization

The adsorption and desorption of nitrogen on each catalyst were measured using a Quadrasorb SI from Quantachrome Instruments. Samples were outgassed under a vacuum at 350 °C overnight and then brought to 77 K via immersion in a liquid nitrogen bath. Total surface area was calculated using multi-point Brunauer–Emmett–Teller (BET) analysis. Pore surface area and pore volume were calculated using Barrett–Joyner–Halenda (BJH) analysis. The t-plot method was used with the DeBoer model for the calculation of the statistical thickness to distinguish the contribution of micropores (<2 nm) to the total surface area.

The composition of the product oil was determined by the pre-calibrated Gas Chromatography-Mass Spectrometer (GC–MS: PerkinElmer GC Claus 680 and MS Clarus SQ 8T) equipped with a Paraffins-Olefins-Naphthenes-Aromatics (PONA) column (Agilent HP-PONA). The oven temperature of the GC was programmed to hold at 35 °C for 15 min, ramp to 70 °C at 1.5 °C/min, rise to 150 °C at 3 °C/min and hold for 30 min, then ramp to 250 °C at 3 °C/min and hold for 2 min.

The water content of liquid sample produced from each run was determined using Karl Fischer (KF) titration (Metrohm 870 Titrino Plus) through averaging the results collected from at least three independent measurements.

The Transmission Electron Microscopy (TEM) spectra were acquired on a Philips Tecnai TF-20 TEM instrument operated at 200 kV. An X-ray analyzer for Energy-Dispersive X-ray (EDX) spectroscopy is incorporated into the instrument for elemental analysis under STEM mode for improving image contrast between C and Ag phases. The sample was first dispersed in ethanol and supported on honey carbon on a 200 mesh Cu grid before the TEM images were recorded.

The X-ray Diffraction (XRD) analysis of the catalysts were carried out on a Rigaku ULTIMA III X-ray diffractometer with Cu Kα irradiation at a voltage of 40 kV and current of 44 mA in the 2θ of 5–80°.

The ^{13}C NMR experiments were conducted at 9.4 T ($\nu_0(^{13}C) = 100.6$ MHz) on a BRUKER AVANCE III 400 spectrometer with a BBFO probe. ^{13}C NMR chemical shifts were referenced to $CDCl_3$ at 77.26 ppm. A spectral width of 26 kHz and a pulse delay of 2 s were used to acquire 17,000 scans per spectrum.

Acidity measurements were performed by NH_3 TPD using ~200 mg samples in an Altamira AMI-390 system. Ammonia was selected due to its simplicity, small molecular size, and ability to

titrate both strong and weak acid sites on the catalyst. Prior to measurements, fresh samples were activated in 10% O_2/He at 600 °C for 30 min with a ramp rate of 10 °C/min. All samples were then cooled to 120 °C for adsorption of ammonia, performed using a flow of 25 sccm of 10% NH_3/He for 30 min. After flowing He for 10 min to remove any physically adsorbed NH_3, TPD was carried out by ramping to 600 °C with at 30 K/min and a hold of 30 min. A thermal conductivity detector (TCD) determined the amount of desorbed NH_3. Upon completion of each experiment, seven pulses of 5 mL of 10%NH_3/He were used to calibrate the TCD response.

The surface acidity of catalyst was also investigated by Diffuse Reflectance Infrared Fourier Transform (DRIFT) spectroscopy of adsorbed pyridine. The DRIFT spectrum was acquired by a Thermo Scientific Nicolet iS50 equipped with an environmental chamber and a liquid-nitrogen cooled mercury–cadmium–telluride (MCT) detector. The gas inlet of a multifunctional reactor system was employed for the gas introduction to DRIFTS via Fluorinated Ethylene Propylene (FEP) tubing (Thermo Scientific, tubing 890 FEP, 8050-0125). The connection between the FEP tubing and the environmental chamber was accomplished through a short tubing with an inside diameter of 1/4 inch. The gas inlet was also connected to a bubbler for liquid feedstock introduction using two three-way valves. Inlet gas could pass through the liquid sample before entering the chamber. For conducting pyridine adsorption, the catalyst sample was first put in the environmental chamber under 30 sccm N_2 flow at 500 °C for 30 min to remove impurities adsorbed onto the catalyst surface during storage before collecting background spectra at room temperature. The N_2 flow was then sent into the aforementioned bubbler filled with pyridine and kept for 10 min in order to introduce pyridine into the environmental chamber as vapor phase. After that, the gas flow was switched back to 30 sccm pure N_2 through bypassing the bubbler. The spectrum was then recorded in an absorbance mode upon stabilization for 30 min at room temperature under 30 sccm N_2. In a similar matter, in-situ DRIFTS study was also conducted during ethanol conversion under various environments when catalyst sample was charged in the chamber and the aforementioned bubbler was filled with ethanol.

Thermographic Analysis (TGA) profiles were used to determine the thermal coke formation as well as the stability of the catalysts, which were crucial to decide the future deactivation study. TGA measurement was fulfilled with a simultaneous thermal analyzer (PerkinElmer STA 6000). The samples were held at 30 °C for 1 min, then heated to 995 °C at a rate of 20 °C/min under 30 mL/min air flow. In addition, the TGA signal along with the simultaneously collected Differential Scanning Calorimetry (DSC) signal from the same instrument were also engaged to study the involved reaction features, which was accomplished through ramping the sample temperature to the destination temperature with a rate of 40 °C/min under 30 mL/min N_2 flow and a hold for 30 min under various gas environments (i.e., N_2 + ethanol vapor or CH_4 + ethanol vapor).

2.3. Performance evaluation

The catalytic test was performed in a fixed-bed continuous-flow stainless steel reactor (i.d., 2.54 cm; length, 61 cm) at atmospheric pressure using a house-made multifunctional reactor system with configuration described in our earlier publication [24]. Ethanol (anhydrous, Green Field) was delivered to the reactor system through a HPLC pump (Series I, Scientific Systems) at flow rate of 0.8 mL/min and turned into vapor phase through an evaporator heated at 150 °C before being sent to the reactor. The feed gases, N_2 (CP grade) and CH_4 (CP grade), were provided by Praxair and used as received. The gas mixture composed of 95% CH_4 and 5% N_2 (internal standard) was introduced into the reactor with a total flow rate of 200 standard cubic centimeter per minute (sccm) controlled by calibrated mass flow meters (Cole-Parmer). H_2 flow (CP grade) was used when mentioned.

In a typical run, catalyst bed (0.25 g) was sandwiched between two layers of quartz wool in the vertically oriented reactor. The reactive gas mixture including methane and ethanol vapor after well mixing was introduced into the reactor by following a down-flow direction. After exposed to the top layer of quartz wool, the gas got in contact with catalyst bed where reaction took place upon heating. The generated gas products exited from the bottom of the reactor after passing through the bottom quartz wool layer which is exclusively used to prevent particle matters from diffusing into the underneath porous frit and thus resulting in its blockage. The reactor was heated by an electric furnace (MTI OTF-1200X-S-VT) at a heating rate of 20 °C·min^{-1} and held at each temperature for 60 min. The temperature range is 300–500 °C. Once the desired temperature was chosen, the reactor was directly heated up to that temperature and held for 3 h. The gas products were analyzed by an on-line four-channel micro-GC (490, Agilent) equipped with thermal conductivity detectors, which can precisely analyze H_2, O_2, N_2, CH_4, and CO in the first channel equipped with a 10 m molecular sieve 5A column; CO_2, C_2H_2, C_2H_4, and C_2H_6 in the second channel installed with a 10 m PPU column; and C_3–C_6 and $C_{3=}$–$C_{5=}$ in the third and fourth channels charged with a 10 m alumina column and a 8 m CP-Sil 5 CB column, respectively. Ar and He are the carrier gases for the first and other three channels, respectively. The liquid products were collected in a cold trap at −5 °C powered by a 50% ethylene glycol-50% DI water cooled chiller (Polyscience LS5), and weighted after each run. The mass and carbon balances counting gas, liquid, and solid (i.e, coke formed on catalyst surface) products were conducted after each run with measured closures of 0.94–0.98 and 0.91–0.96, respectively.

In order to save the usage of $^{13}CH_4$, the isotopic labeling experiment was conducted using a 100 mL Parr® reactor under batch mode. The same amount of catalyst (0.25 g) was charged into the reactor filled with ethanol vapor and $^{13}CH_4$ at 1 atmospheric pressure. The reactor temperature was then ramped up with a rate of 20 °C/min to the destination temperature (400 °C) and held for 30 mins. Upon the reaction completion, the reactor was allowed to cool down to room temperature before product collection. The formed liquid product embedded into the charged solid catalyst was extracted out using CS_2 (GC grade, EMD Chemicals) as solvent and internal standard for following NMR analysis. In a similar matter, non-isotopic labelled methane run was performed as the reference.

The liquid and oil yields as well as liquid product selectivity reported in this paper are calculated by following the equations below:

$$\textit{Liquid Yield\%} = \frac{\textit{weight of collected liquid in the condenser}}{\textit{Weight of the fed ethanol}} \times 100.$$

$$\textit{Liquid Product Selectivity\%} = \frac{\textit{weight of collected liquid product the condenser}}{\textit{Weight of the converted ethanol}} \times 100.$$

$$\textit{Oil Yield\%} = \frac{\textit{weight of collected liquid} - \textit{water weight measured through KF titration}}{\textit{Weight of the fed ethanol}} \times 100.$$

Table 1
Ethanol conversion, liquid product selectivity, and liquid yield from the runs over 5%Zn/ZSM-5 at various reaction temperatures and 1 atm under methane environment.

		Reaction Temperature (°C)		
		300	400	500
Selectivity (wt.%)	Ether	93.85	95.20	29.42
	Acetone	5.92	0.28	54.73
	Ester	0.10	0.54	0.00
	Acetic acid	0.00	0.33	12.50
	Cyclopentene	0.00	0.76	3.35
	Aromatics	0.08	0.94	0.00
	Aldehyde	0.03	1.95	0.00
Ethanol Conversion (%)		63.14	71.39	6.56
Liquid yield (wt.%)		81.45	30.06	41.08

Table 2
Ethanol conversion, liquid product selectivity, and liquid yield from the runs over 1%Ag-5%Zn/ZSM-5 at various reaction temperatures and 1 atm under methane environment.

		Reaction Temperature (°C)		
		300	400	500
Selectivity (wt.%)	Ether	95.72	77.40	53.35
	Acetone	2.88	17.78	6.52
	Ester	0.00	0.72	0.78
	Acetic acid	0.00	0.77	9.06
	Cyclopentene	0.00	0.79	13.87
	Aromatics	1.40	0.86	0.57
	Aldehyde	0.00	1.67	15.85
Ethanol Conversion (%)		24.29	44.20	68.12
Liquid yield (wt.%)		84.05	69.12	23.55

Table 3
Ethanol conversion, liquid product selectivity, and liquid yield from the runs over 1%Ag/ZSM-5 at various reaction temperatures and 1 atm under methane environment.

		Reaction Temperature (°C)		
		300	400	500
Selectivity (wt.%)	Ether	97.39	62.79	51.75
	Acetone	2.18	3.39	42.79
	Ester	0.25	0.56	0.00
	Acetic acid	0.00	0.33	0.99
	Cyclopentene	0.00	0.00	0.00
	Aromatics	0.19	32.92	4.19
	Aldehyde	0.00	0.00	0.27
Ethanol Conversion (%)		51.38	51.60	29.12
Liquid yield (wt.%)		80.35	35.08	37.80

3. Results and discussion

3.1. Catalytic performance

3.1.1. Effect of reaction temperature

The reaction performances of 5%Zn/ZSM-5, 1%Ag-5%Zn/ZSM-5, and 1%Ag/ZSM-5 were evaluated and their catalytic effects on liquid product formation from ethanol and methane interaction are summarized in Tables 1–3 , respectively. The liquid yield is notably reduced along with the increase of reaction temperature, particularly from 300 °C to 400 °C no matter what catalyst is charged except for the 500 °C runs over 5%Zn/ZSM-5 and 1%Ag/ZSM-5, which might be because higher reaction temperature favors the ethanol cracking and thus leads to more gas formation which is verified by the increased total product gas flow rate (not shown). The collected liquid products from three runs were also further analyzed using GC–MS for composition determination, the results of which are also listed in Tables 1–3. For the ease of data interpretation, the more than 60 detected compounds are classified into 8 individual groups. Ethylidene diethyl ether (i.e., 1,1-diethoxyethane) and ethylene glycol diethyl ether (i.e., 1,2-diethoxyethane) are two major compounds identified in the ether category along with certain amount of diethyl ether and occupy more than 90% of total ether counted, implying that dehydration and dehydrogenation between three ethanol molecules might take place to a notable degree and play a competing role with aromatization reaction after taking their high concentrations in the collected liquid product into the consideration. The acetone formation might originate from the aldol condensation of two acetaldehyde molecules formed from dehydrogenation of ethanol [28]. Song, et al. also suggested in the same paper that the observed acetic acid production might be derived from the oxidation of the adsorbed acetaldehyde molecule by the surface oxygen available in the charged catalyst. The well-known Fischer esterification of ethanol and acetic acid in the gas phase might account for the generation of trace amount of ethyl ester, the dominating ester species in the product oil. The unnegligible cyclopentene formation (mainly 2-cyclopenten-1-one, 2-methyl) observed over Ag-Zn/ZSM-5 at 500 °C might come from the dehydrocyclization of ethanol. The same run also witnesses the production of aldehyde with carbon chain length ranging from 4 to 6 at 500 °C such as 2-butenal, the major species identified in this category, which might result from the dehydration and dehydrogenation reactions between two ethanol molecules.

From the catalytic performance comparison between these three runs, it is easy to conclude that Zn addition favors low temperature dehydration and dehydrogenation of ethanol, thus leading to the formation of the most abundant ether species at 400 °C (Table 1). On the other side, Ag introduction benefits the aromatization of ethanol, thus generating the highest amount of aromatics at 400 °C (Table 3). The co-existence of Ag and Zn yields the synergetic effect on assisting C—C bond cleavage of ethanol to produce gas species, as evidenced by the lowest liquid yield observed at 500 °C (Table 2). Since the focus of this study is the co-aromatization of methane and ethanol, 1%Ag/ZSM-5 as the favored catalyst and 400 °C as the preferred reaction temperature are selected with the most interest for further investigation.

Table 4
Ethanol conversion, liquid product selectivity, and liquid yield from various runs at 400 °C and 1 atm under methane environment.

		Selectivity (wt.%)		
		1%Ag/ZSM-5	HZSM-5	No catalyst
Compound	Ether	9.73	16.19	98.47
	Acetone	0.78	3.31	1.17
	Ester	0.45	0.3	0.14
	Acetic acid	0	0	0
	Cycloalkene	1.71	3.64	0
	Aromatics	86.85	75.38	0.2
	Aldehyde	0.48	1.12	0
Ethanol Conversion (%)		75.43	46.19	55.68
Liquid yield (wt.%)		26.13	33.52	83.6

3.1.2. Effect of catalyst addition

The catalytic effect of Ag/ZSM-5 is further evaluated directly at 400 °C without first undergoing 300 °C test and the results are shown in Table 4. For better illustration of the catalyst effect and the role played by the loaded active metal (i.e., Ag), the performances from the runs without catalyst addition and without Ag loading are also included into the same table. It is clearly noticed that aromatics appear to form when catalyst is charged and its produc-

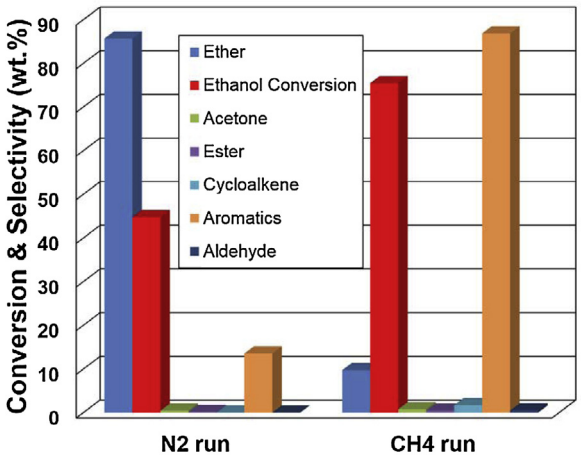

Fig. 1. The ethanol conversion and liquid product selectivity from the runs over 1%Ag/ZSM-5 at 400 °C under N_2 and CH_4 environments.

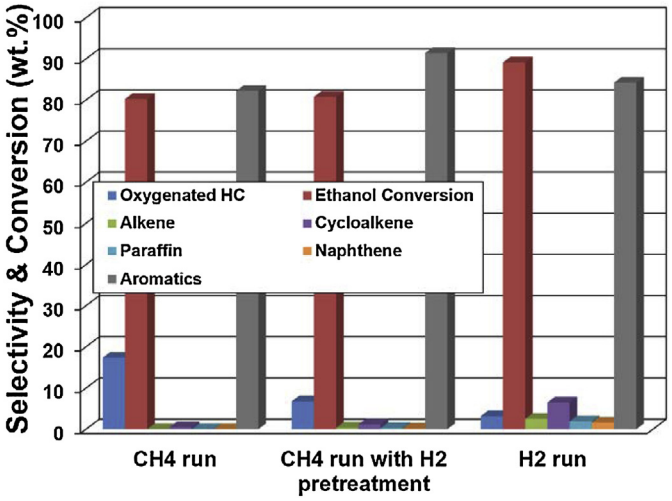

Fig. 2. The ethanol conversion and liquid product selectivity from the runs over 1%Ag/ZSM-5 with and without H_2 pretreatment at 400 °C under CH_4 and H_2 environments.

tion is boosted from 75.4 wt.% to 86.8 wt.% if Ag is introduced into the ZSM-5 framework accompanied with the significantly reduced ether formation and enhanced ethanol conversion, further evidencing that Ag/ZSM-5 is good at aromatics formation and both ZSM-5 support and Ag as active metal contribute to the production of aromatics. After a closer look at the liquid composition (including the unconverted ethanol) difference between Ag/ZSM-5 and HZSM-5 runs, the fact that the increased concentration of aromatics is well followed by the reduced ethanol content when 1%Ag is added while the contents of other species remain almost unchanged suggests that ethanol aromatization might proceed without taking other reported groups of species as reaction intermediates and Ag introduction would mainly facilitate ethanol aromatization and/or help methane activation and dehydroaromatization. In addition, it is worth noting that the notable performance differences between two 400 runs listed in Tables 3 and 4, separately, over Ag/ZSM-5 might be because there are some surface species formed on the catalyst during 300 °C run and left over on the catalyst surface when temperature is raised up to 400 °C and generates some detrimental effect on ethanol aromatization (e.g., blockage of the surface sites for catalyzing aromatization reaction).

3.1.3. Effect of methane presence

The positive effect of methane introduction on aromatics formation is evaluated through performing a similar run under N_2 environment, the results of which are depicted in Fig. 1. The huge jump of aromatics selectivity in the collected liquid product from ~13.5 wt.% to 86.8 wt.% is clearly observed along with notably enhanced ethanol conversion and ether reduction when methane is present in the gas environment, implying that methane might either participate in the dehydroaromatization reaction or provide assistance on ethanol aromatization. The dramatically increased water content in the water layer of the liquid product from 2.8 wt.% to 74.9 wt.% further evidences the boosted degree of ethanol aromatization upon methane presence.

3.1.4. Effect of H_2 pretreatment

In order to determine the oxidation state of Ag for better triggering ethanol aromatization and/or methane activation and dehydroaromatization reaction, the Ag/ZSM-5 catalyst was pretreated by 5% H_2/N_2 flow at 200 sccm and 400 °C for 1 h for completely reducing Ag to its metallic form. Fig. 2 is drawn for better performance comparison between two runs charged with Ag/ZSM-5 catalyst with and without H_2 pretreatment. In addition, the performance collected from a H_2 run (i.e., aromatization of ethanol under H_2 environment) is also included as a reference. The increase of aromatics formation is witnessed along with enhanced ethanol conversion and reduced oxygenated hydrocarbons production when the H_2 pretreated catalyst is engaged, which is even better than that from the H_2 run in term of aromatics selectivity. More importantly, the oil yield is also increased from ~6.6 wt.% to 11.1 wt.% upon H_2 treatment, implying that metallic Ag might be the active site for catalyzing aromatization reaction. After a closer look at the liquid product compositional distribution of various runs and its evolution upon H_2 pretreatment and engagement of H_2 as the gas feedstock, a hypothetic reaction pathway for ethanol aromatization is proposed below, which needs further investigation.

$$Ethanol \xrightarrow{Dehydration} Oxygenated\ HC \xrightarrow{Hydrodeoxygenation} Alene \xrightarrow{Cyclization} Cycloalkene \xrightarrow{Aromatization} Aromatics$$

3.1.5. Proof of methane participation

For further verifying the engagement of methane into the aromatization reaction, the aromatics contained in the liquid product collected over Ag/ZSM-5 with and without H_2 pretreatment under methane environment is compared to those collected from the run where H_2 is employed as the gas feedstock in term of its carbon distribution, the results of which are presented in Fig. 3. Benzene is the only product falling into the C_6 category, which is also true for toluene in C_7 category. Ethyl benzene and xylene are the products observed in C_8 group, among which *p*-xylene and *o*-xylene are the major components with the highest population. C_9–C_{13} groups include the species with methyl, ethyl, propyl, butyl groups, or their combinations attached to benzene and naphthalene as well as small amount of indene derivatives. Fig. 3 witnesses the carbon number distribution peak shifting to the higher end when methane is present, indicating that methane might participate into the aromatization reaction and thus lead to the increased carbon number in the produced aromatics when H_2 run is referred. Moreover, the fact that even higher carbon number shift in the aromatics when the Ag/ZSM-5 catalyst is charged without H_2 pretreatment might suggest that partially reduced Ag (i.e., Ag^+/Ag) as the active site is more efficient in triggering the methane activation and following dehydroaromatization reaction than pure metallic Ag.

In addition, the compositions of gas products from both methane and N_2 runs are also compared to identify the methane contribution

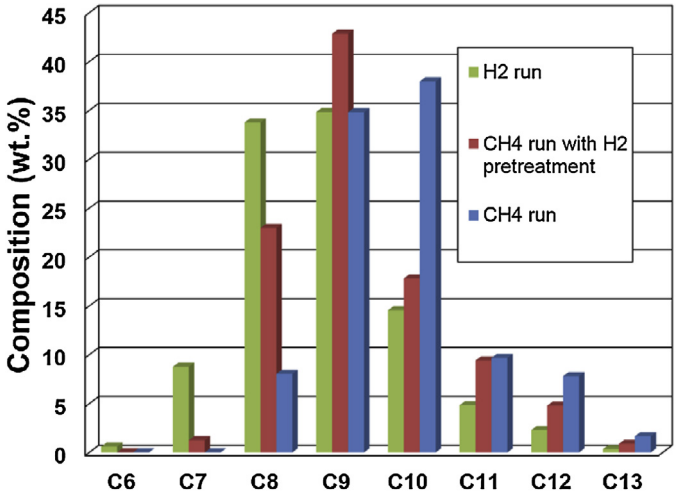

Fig. 3. The carbon number distribution in the aromatics portion of the liquid product collected over 1%Ag/ZSM-5 with and without H_2 pretreatment at 400 °C under CH_4 and H_2 environments.

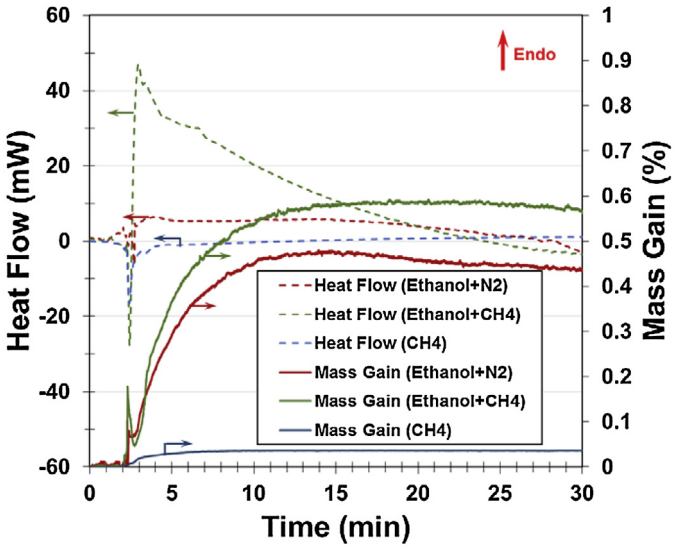

Fig. 4. The TGA-DSC profiles collected over 1%Ag/ZSM-5 during ethanol aromatization under various environments and methane-alone run at 400 °C and 1 atm.

Table 5
Gas product selectivity from the runs collected over 1%Ag/ZSM-5 at 400 °C and 1 atm under various environments.

Gas Environment	Gas Product Selectivity (%)								
	H_2	CH_4	CO	C_2H_4	C_2H_6	C_3	C_4	C_5	C_6
N_2	7.81	4.71	5.52	49.14	1.28	20.75	7.88	1.86	0.81
CH_4	12.62	–	0.45	34.47	5.66	26.52	12.70	3.98	3.51

to the ethanol conversion reaction in the gas phase. As reported in Table 5, a series of hydrocarbons are formed along with H_2 and CO, among which ethylene has the highest selectivity in both runs, indicating the ethanol dehydration reaction taking place to a great level. CO and CH_4 formations are mainly derived from the C—C breakage of ethanol molecule. H_2 production might majorly originate from ethanol and methane aromatization. The higher H_2 selectivity observed over methane run probably suggests the participation of methane into the aromatization reaction. Moreover, it is worth noting that methane run exhibits higher selectivity towards higher hydrocarbons (i.e., C_3–C_6) compared to its N_2 counterpart, implying the methane incorporation into the product molecules similar to what is observed in Fig. 3. The formation of more saturated hydrocarbons such as ethane from methane run supplies an additional clue for methane engagement. Besides, ~6.5% methane conversion is also observed during the methane run after performing a careful composition analysis of the gas product, thus providing another indirect evidence for methane involvement into the reaction.

The methane engagement into the ethanol aromatization reaction with Ag/ZSM-5 charged is further investigated through employing TGA-DSC, the result of which is displayed in Fig. 4. For better comparison, the results collected from its N_2 counterpart and the methane-alone run are also included. When the data of mass gain from three runs are compared, a strongest peak is clearly observed at around 2.5 min and followed by a gradual mass gain with higher rate to reach a higher plateau over ethanol + methane run. The initial jump in mass gain might result from the adsorption of gas reactants. Compared to that from N_2 run, more than doubled mass gain boost over methane run might suggest the adsorption of methane molecules on the catalyst surface under the assistance of co-present ethanol since methane alone is very hard to be chemically adsorbed due to its highly symmetric molecular structure which leads to no polarity for electron attack as discussed in the introduction section and evidenced from the complete disappearance of such peak in the TGA profile collected over methane-alone run. The rapid drop in mass gain immediately after the jump observed during ethanol conversion under various environments indicates certain chemical reaction taking place, thus resulting in the desorption of formed products from the catalyst surface. The following increase in mass gain probably originates from the accumulation of surface intermediates and/or coke formation on the catalyst surface. Therefore, higher mass gain over methane run might imply more coke formation. Such observations are consistent with what are noticed in DSC signals collected from these two runs when ethanol is present in the gas phase as feedstock. The initial negative peak suggests the exothermic feature due to the adsorption of gas reactants. The more prominent negative peak from ethanol + methane run might also evidence the co-adsorption of methane on the catalyst surface along with ethanol. A much stronger positive peak is clearly witnessed over ethanol + methane run when that from its N_2 counterpart is referred, indicating more endothermic feature occurring from the interaction between methane and ethanol molecules. According to the thermodynamic calculation with all reactants and products in the gas phase, ethanol aromatization reaction has a reaction heat of 19.15 kcal/mol while ethanol and methane co-aromatization reaction demonstrates a much higher endothermic feature at 58.57 kcal/mol. Therefore, such notably promoted increase in positive heat flow over ethanol + methane run may provide another evidence of methane participation into the ethanol aromatization reaction. Furthermore, the synergetic effect occurring between ethanol and methane molecules is further witnessed when the almost zero DSC signal from methane-alone run is cited after an initial exothermic feature. In addition, the gradual decline in heat flow with increasing time noticed during ethanol conversion under different gas atmospheres is probably attributed to the catalyst deactivation due to coke deposition when TGA signals are cited in the same time frame.

In order to provide a more direct evidence of methane participation into the ethanol aromatization reaction, $^{13}CH_4$ was employed as the methane source for conducting ethanol conversion under the facilitation of Ag/ZSM-5 catalyst and the obtained liquid product underwent NMR analysis. The resulting ^{13}C NMR spectra is shown in Fig. 5a. For better comparison, the result collected from the non-isotopic labelled run is also included. The huge peak centered at 192.6 ppm belongs to the CS_2 which serves as a solvent for liquid product extraction from the charged solid catalyst and internal

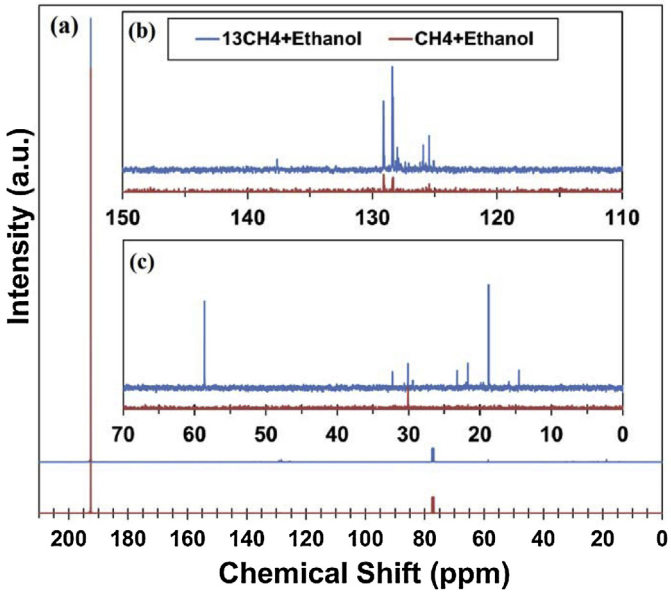

Fig. 5. (a) The ^{13}C NMR spectra and its zoom-in views at chemical shift region of (b) 110–150 ppm and (c) 0–70 ppm of the liquid products collected from ethanol conversion under $^{13}CH_4$ and CH_4 environments, respectively, at 400 °C and 1 atm.

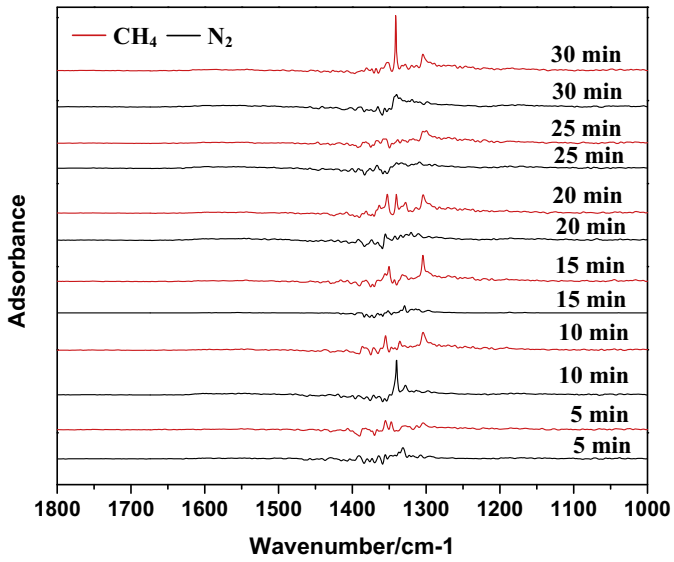

Fig. 6. The DRIFT spectra collected at different time over 1%Ag/ZSM-5 during ethanol conversion under various environments at 400 °C and 1 atm.

standard for more accurate NMR comparison. As mentioned in the experimental section, the peak located at 77.3 ppm is due to the presence of $CDCl_3$ introduced for instrumental calibration. For better illustrating the difference in ^{13}C NMR response from the liquid products formed from two runs, the zoom-in views of Fig. 5a at two different chemical shift regions are also present in Fig. 5b and c. The notable increase (by 3.3 times) in ^{13}C signals resulting from carbon in aromatic rings formed from the $^{13}CH_4$ + ethanol run is clearly witnessed in Fig. 5b compared to that from its non-isotopic labelled counterpart, strongly indicating the methane involvement into the ethanol aromatization reaction. After a closer look at the zoom-in spectra, there are four major peaks recognized from the background noise in the ^{13}C NMR spectra of the liquid product obtained from CH_4 + ethanol run. The peaks at 129.2 ppm and 127.9 ppm are assigned to the benzene ring carbon atoms that are on the ortho and meta positions of the alkyl substituent, respectively [29]. The signal at 125.4 ppm is due to the benzene ring carbon atoms that are on the para position of the alkyl substituent. The one at 30.5 ppm in Fig. 5c belongs to the carbon on the benzylic site of the alkyl substituent. More peaks are observed with an improved signal to noise ratio when $^{13}CH_4$ is employed. Besides the peaks at the aforementioned regions, the peak due to the benzene ring carbon that is directly bonded to the alkyl substituent and expected with a chemical shift around 137 ppm is present on the $^{13}CH_4$ + ethanol spectrum (Fig. 5b). However, its intensity is fairly low, indicating that this carbon site might not be favored for methane incorporation. Furthermore, the non-uniform distribution of ^{13}C signal at various carbon positions of benzene ring suggests that ethanol and methane might jointly provide the building blocks for benzene ring construction and subsequent aromatics formation. In addition to the signal due to aromatic carbons, peaks at 58.6, 30.5, 23.2, 21.7, 18.8 and 14.5 ppm are also observed in Fig. 5c over $^{13}CH_4$ + ethanol run. The 58.6 ppm peak should be derived from the carbon atoms, which are bonded to oxygen directly, of ethers when the liquid product distribution from this run is referred in Fig. 1, implying that methane might participate in the etherification reaction. The rest of the peaks can be partially attributed to the other alkyl carbon atoms of ethers. The great portion of these ^{13}C signals should originate from the alkyl substituent carbon atoms, which attach to the phenyl ring as side chain in the formed aromatics, thus providing a direct experimental evidence to support our aforementioned interpretation on the increased average carbon number in the produced aromatics collected from methane run as shown in Fig. 3.

3.2. Characterization of the catalysts

In order to identify the correlation between the physical properties of the catalysts and their catalytic performances, versatile characterization techniques including N_2 physisorption, XRD, TEM, DRIFTS, NH_3 TPD, and TGA have been employed in this study. The porous properties of various catalysts are analyzed through N_2 physisorption and the results are reported in Table 6. Compared to pure HZSM-5 support, Ag and/or Zn modified zeolite catalysts have increased total surface area, reduced pore volume and pore size to certain degrees. The highest total surface area and least reductions in pore volume and pore size are observed over Ag/ZSM-5, which might be related to its better aromatization performance. In addition, it is worth noting that upon metal loading catalyst's external surface area is greatly reduced but compensated by the increased internal surface area. Ag/ZSM-5 is embedded with the highest internal surface area, thus benefiting the aromatization reaction taking place within the zeolite pores where active metal is well dispersed, particularly when its highest pore volume and pore size among those of three tested catalysts are taken into consideration, which grants gas reactants more accessibility for in-pore reaction.

In order to further identify the location where aromatization reaction takes place on the catalyst's surface, the ethanol surface conversion reaction under various environments was in-situ monitored by DRIFTS at 400 °C and the collected spectra are presented in Fig. 6 along with reaction time. No nonnegligible IR vibration peaks are detected in the 1500–1700 cm^{-1} region of all spectra included where characteristic aromatic C=C bond bending features should appear [30] if there is detectable amount of aromatics formed on the external surface of the charged Ag/ZSM-5 catalyst, indicating that aromatization reaction might mainly take place within the zeolite pores where are difficult to be illuminated by IR beam. In addition, the multiple IR peaks present in the 1000–1500 cm^{-1} region are derived from the C—O stretching and C—H bending, indicating the interaction between adsorbed ethanol and the catalyst surface [28].

The XRD patterns of H-ZSM-5, 5%Zn-1%Ag/ZSM-5, 5%Zn/ZSM-5, and 1%Ag/ZSM-5 at various life stages are presented in Fig. 7. The 5%Zn-1%Ag/ZSM-5 obtained by loading of 1 wt.% Ag and 5 wt.% Zn

Table 6
The porous properties of various catalysts.

Samples*	BET Surface Area (m^2/g)			Porous Volume (cm^3/g)			Pore Size (Å)
	External	Microporous	Total	Microporous	Mesoporous	Total	
Pure ZSM-5	125.7	235.6	361.4	0.124	0.196	0.321	15.6
Ag/ZSM-5	64.7	353.3	418.0	0.142	0.099	0.241	13.1
Ag-Zn/ZSM-5	69.6	320.9	390.6	0.127	0.084	0.211	9.9
Zn/ZSM-5	57.5	310.9	368.4	0.124	0.082	0.206	9.9

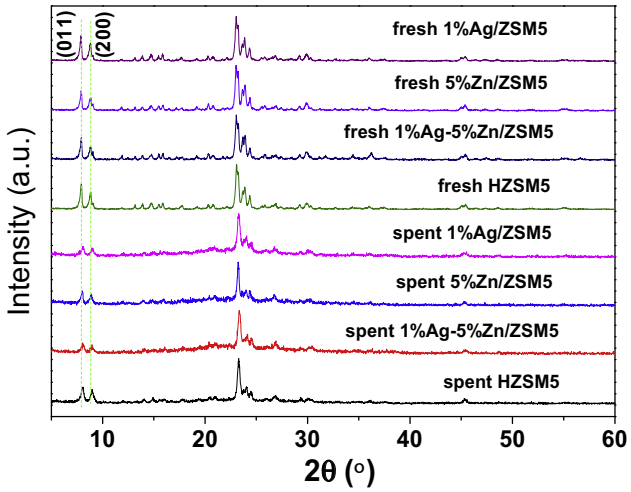

Fig. 7. XRD patterns of fresh and spent HZSM-5, Zn/ZSM-5, Ag-Zn/ZSM-5, and Ag/ZSM-5 catalysts.

on H-ZSM-5 does not show any additional peak besides those of ZSM-5 framework, indicating that the silver and zinc species are highly dispersed at the surface and/or in the channel of zeolite support. Similarly, the zinc and silver species are also highly dispersed on/in 5%Zn/ZSM-5 and 1%Ag/ZSM-5, respectively. According to our previous study [24], highly dispersed metal species are active for catalyzing CH_4 to be incorporated into the carbon chain of the bio-oil and enhancing the quantity of the produced bio-oil. Therefore, the highly dispersed Zn and Ag species would benefit the achievement of better catalytic performance. After a careful comparison, it is also noticed that upon the introduction of Ag and/or Zn species into the HZSM-5 framework, the intensity of the diffraction peaks due to (011) and (200) crystal planes are significantly reduced. A plausible explanation is that the doped Ag and/or Zn species migrate into the HZSM-5 framework and reduce the crystalline of (011) and (200) planes. In addition, the reaction does not make notable change in the crystal structure of three engaged catalysts, which is supported by the fact that the zeolite framework is well maintained and no additional peaks appear due to new phase formation and/or active metal sintering when the XRD patterns collected over the spent catalysts are referred in Fig. 7.

Besides XRD patterns released in Fig. 7, the samples are further investigated by employing TEM technique. From the TEM image of fresh 1%Ag/ZSM-5 in Fig. 8, silver particles (the near spherical particle in the image whose composition is confirmed by performing an EDX analysis at several selected spots) are widely dispersed throughout the whole surface of the ZSM-5 support with averaged diameter of ~2 nm. The morphology of the spent catalyst after the reaction with ethanol under CH_4 environment is also investigated. The crystalline of the catalyst framework stays intact and the fringe of the zeolite structure is still clearly observed even after reaction

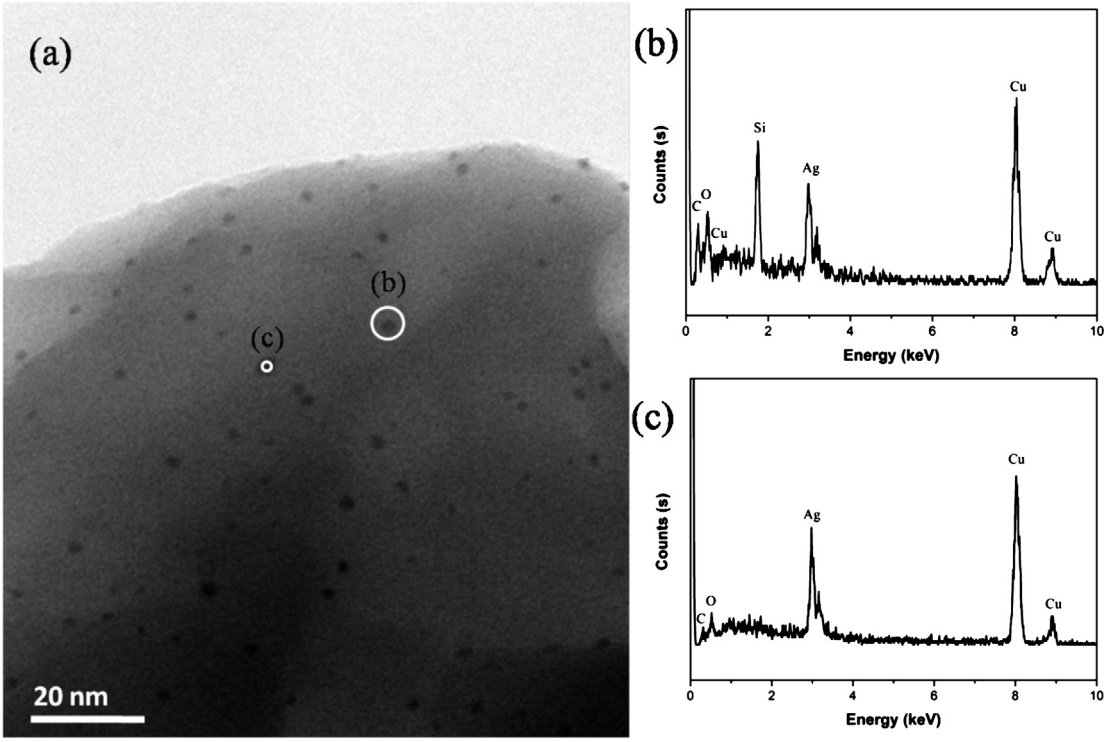

Fig. 8. TEM image of the Ag/ZSM-5 catalyst (a) and the corresponding EDX spectra at spot (b) and (c) selected in (a).

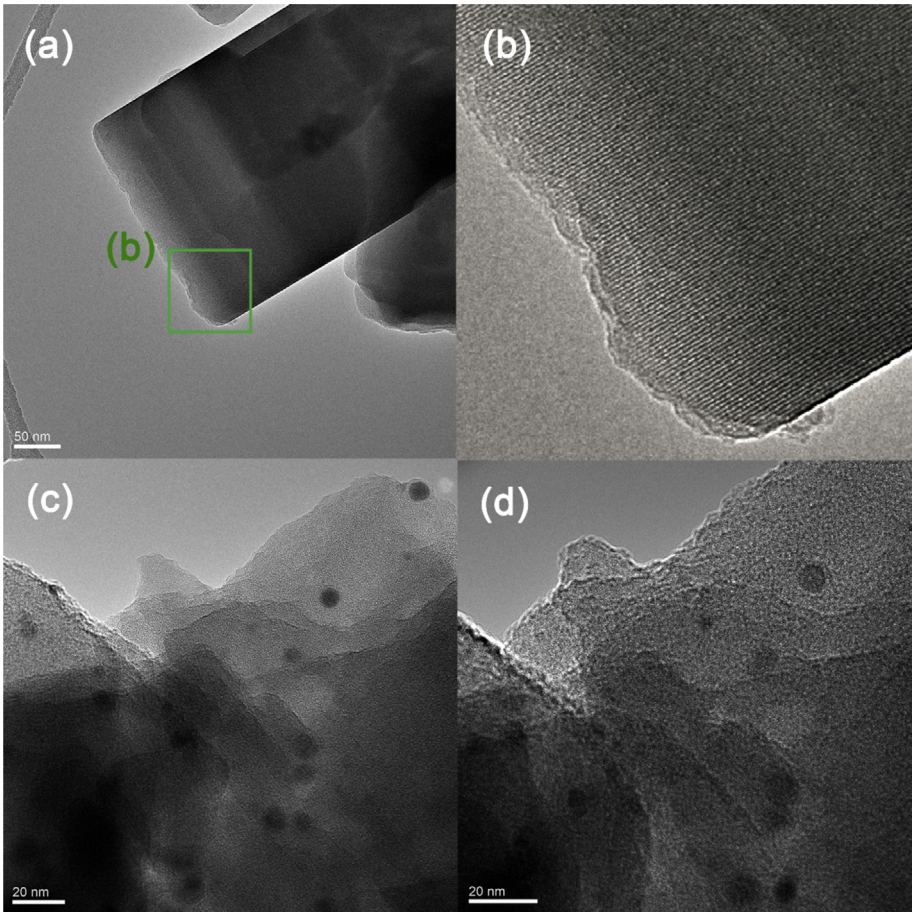

Fig. 9. TEM Images of spent Ag/ZSM-5 catalyst (a) with ZSM-5 support focused, (b) zoom-in view of the squared area in (a), (c) and (d) with active metal focused at different resolutions.

(Fig. 9a and b). Fig. 9c and d shows the TEM images of one representative area of the spent catalyst at two different magnifications. The averaged size of these particles is determined to be 8 ± 1.5 nm after investigating the TEM images taken from various spots of the spent sample, which is larger than that of fresh catalyst, indicating that the dispersion of the metal species gets worsen and particle agglomeration occurs to certain degree after the reaction under methane environment.

When the TEM image of the fresh Ag-Zn/ZSM-5 catalyst is referred (Fig. 10a), it is observed that two types of particles are well dispersed on/in the ZSM-5 zeolite support. The darker particles with bigger sizes (about 10–20 nm) are supposed to be Ag_2O, while the lighter particles with much smaller sizes (<5 nm) should be ZnO, which has been confirmed by the EDX analysis, the results of which are shown in Fig. 10b and c. It is witnessed from Fig. 10a and b that only Ag signal is detected (by EDX) when the selected area contains darker particle with bigger size. In Fig. 10a and c, no Ag signal is detected (by EDX) when the selected area does not contain any bigger and darker particles, and just Zn signal is noticed due to the presence of ZnO particles recognized from its smaller and lighter features in the corresponding TEM image. These results confirm that the bigger and darker particles are Ag_2O, while the smaller and lighter particles are ZnO.

After the ethanol reaction under methane environment, the spent Ag-Zn/ZSM-5 catalyst is also further studied using TEM technique. The framework of ZSM-5 support is well maintained as evidenced in the intact fringe structure (not shown) and the averaged particle size of the loaded active metals is 12.8 ± 3.2 nm after analyzing TEM images collected at different spots like the one shown in Fig. 11a. The elemental composition of the detected particle dispersed on the spent catalyst surface is further measured using EDX spectroscopy. As shown in Fig. 11a and b, the almost spherical particle which is probably covered by a thin layer of carbon deposition is determined to be sliver clusters. Zn signal is observed when the EDX detector is focused on the ZSM-5 framework without recognizable particles as shown in Fig. 11c, implying that Zn might be highly dispersed inside the zeolite porous structure which is beyond the detection limit of the engaged TEM instrument. Therefore, it is concluded that the relatively larger Ag particles might partially account for the relatively poor aromatization capability of Ag-Zn/ZSM-5 catalyst.

The highly dispersed Zn particles are further observed when fresh Zn/ZSM-5 is analyzed using TEM-EDX and results are reported in Fig. 12. No recognizable metal particles are identified after a thorough morphology scan as evidenced by the TEM image shown in Fig. 12a. The corresponding EDX spectra at two randomly chosen spots as indicated in Fig. 12a are displayed in Fig. 12b and c, indicating the presence of Zn throughout the whole zeolite surface.

The surface acidity of various catalysts used in this study is also calibrated by choosing pyridine as the probe. Fig. 13 shows the DRIFT spectra collected over HZSM-5, Ag/ZSM-5, Zn/ZSM-5 and Ag-Zn/ZSM-5 upon the adsorption of pyridine at room temperature. The peaks at around 1450 cm^{-1} are assigned to Lewis acid sites [31,32], while those appearing at 1540 cm^{-1} are due to Brösted acid sites [33] upon pyridine adsorption. It is noticed that the Lewis acid sites are observed on HZSM-5, Ag/ZSM-5, Zn/ZSM-5 and Ag-Zn/ZSM-5. However, the peak intensity over Zn/ZSM-5 and Ag-Zn/ZSM-5 is much weaker, indicating that the number of Lewis

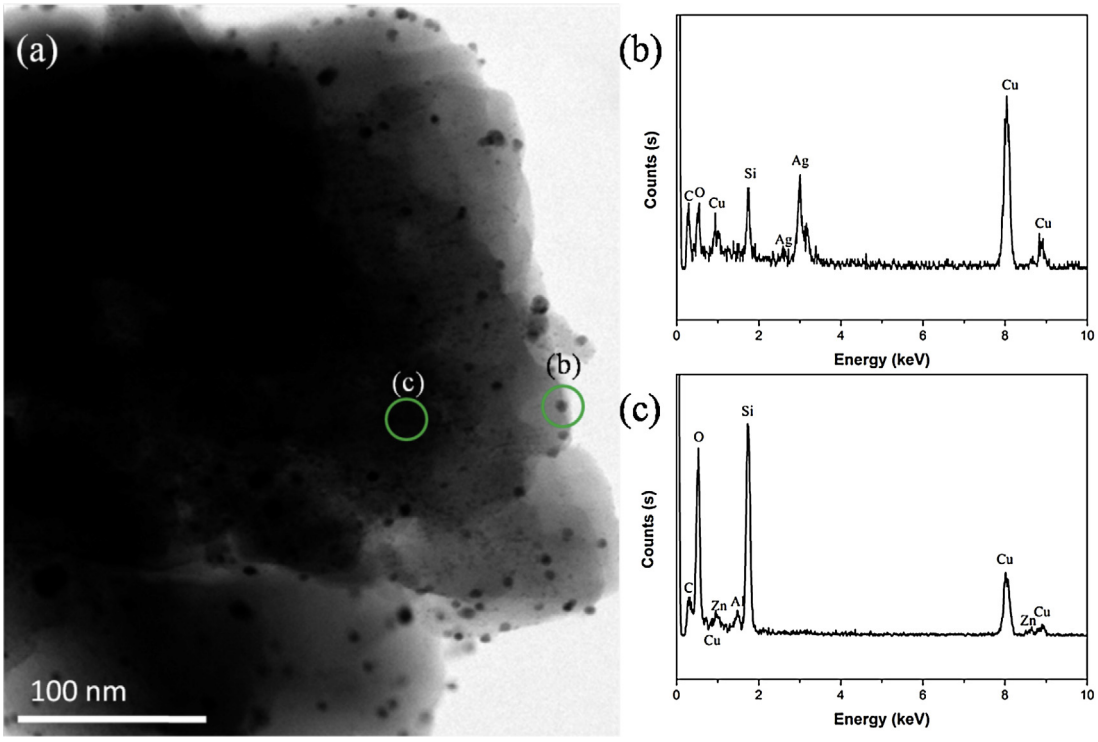

Fig. 10. TEM image of the fresh Ag-Zn/ZSM-5 catalyst (a) and the corresponding EDX spectra at spot (b) and (c) selected in (a).

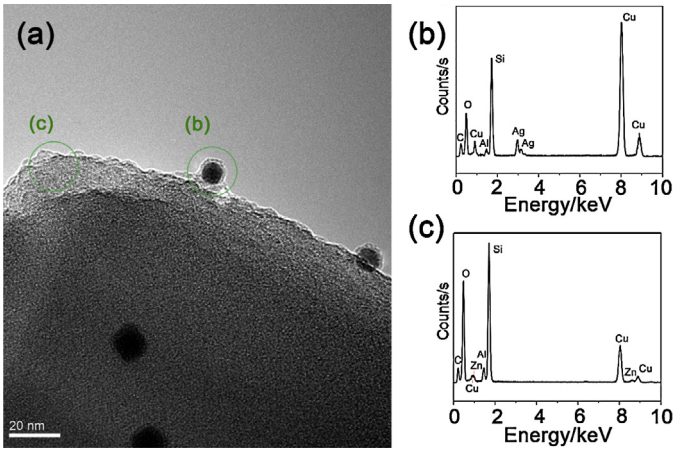

Fig. 11. TEM Image of spent Ag-Zn/ZSM-5 catalyst (a) with active metal particles focused, and the corresponding EDX spectra at spots (b) and (c) selected in (a).

acid sites is notably smaller on these two catalysts. Combined with the TEM studies (Figs. 11 and 12), the observations suggest that the highly dispersed Zn particles might locate themselves on the surface acidic sites, resulting in the significant suppression of the acidic sites abundance on the catalyst surface. The presence of Brösted acid sites on HZSM-5 and Ag/ZSM-5 are evidenced by the peaks at 1540 and 1546 cm^{-1}. The other peaks identified in the spectra of these two catalysts are also closely associated to the Brösted acid sites. The peaks at around 1490 cm^{-1} are assigned to the 19a mode of pyridinium H-bonded with pyridine as well as the ZSM-5 framework. The peaks centered at ~1600 cm^{-1} are attributed to the hydrogen-bonded pyridine. The peaks at around 1640 cm^{-1} are due to the 8a and 8b mode of pyridinium H-bonded with pyridine and the ZSM-5 framework [34], where the noted 8a, 8b, and 19a are the mode symbols [35,36]. The strong Lewis and Brösted acidity of Ag/ZSM-5 may be closely related to its good catalytic performance towards aromatization, since it has been numerously reported in the literature that the abundant Lewis and Brösted surface acid sites are highly responsible for the dehydration, dehydrogenation, and aromatization of ethanol and methane to produce aromatics [37].

The features of surface acidic sites of various catalysts developed in this study are further analyzed using NH_3 TPD, the results of which are displayed in Fig. 14 for better comparison. The low-temperature (LT) peak ranging from 200 to 400 °C might originate from the NH_3 molecules desorbed from the weak surface acidic sites and the high-temperature (HT) peak spanning from 400 to 600 °C is probably associated with NH_3 molecules desorbed from strong surface acidic sites [38,39]. The LT peak is observed over all the tested samples with Ag/ZSM-5 catalyst showing less peak area, implying less week acidic sites present on the surface of Ag/ZSM-5 catalyst. Nevertheless, the notable HT peak is only witnessed when Ag/ZSM-5 is charged, indicating that strong Brösted and Lewis acid sites are also available [38] on Ag/ZSM-5 surface and responsible for catalyzing methane and ethanol aromatization reactions as suggested by the previous researches [40,41]. In addition, after quantification, the total acid amounts for Ag-Zn/ZSM-5, Zn/ZSM-5, Ag/ZSM-5, and Ag/ZSM-5 after H_2 treatment are determined to be 1429, 1356, 1193, and 1171 μmol NH_3/g_{cat}, respectively. Combined with the strength of surface acidic site, it might be concluded that more abundance of strong surface acidic sites benefits aromatics formation during ethanol conversion under methane environment.

The carbon deposition on various spent catalysts is investigated through employing TGA and their results are compiled in Fig. 15, based on which the averaged coke formation rates from various runs are calculated in Table 7. It is worth noting in Fig. 15a that the degree of mass loss for each spent catalyst upon heating under air flow correlates well with its catalytic performance towards aromatics formation when Tables 1–4 are referred. In other words, it seems that better aromatization activity trends to form more coke on the catalyst surface, which is further evidenced when Fig. 15b is taken into consideration. The notably less coke is produced when 1%Ag/ZSM-5 is charged under N_2 environ-

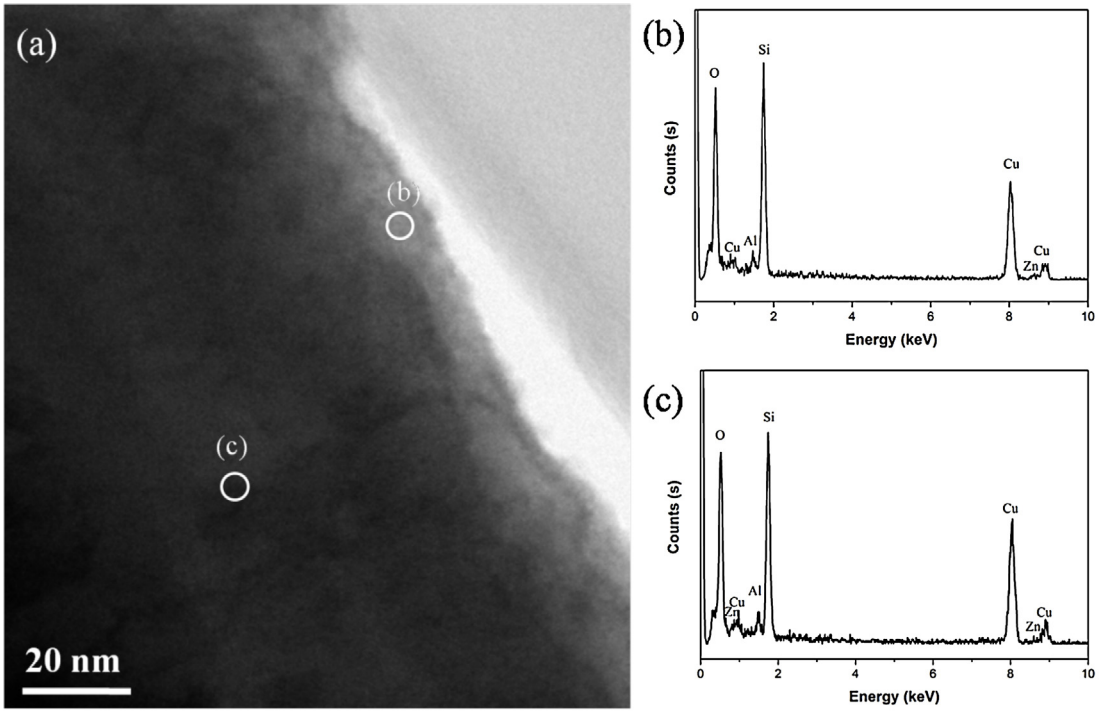

Fig. 12. TEM image of the fresh Zn/ZSM-5 catalyst (a) and the corresponding EDX spectra at spot (b) and (c) selected in (a).

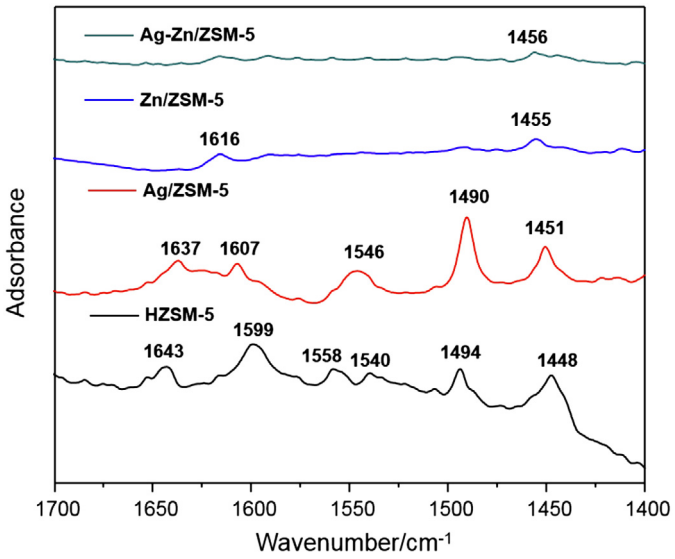

Fig. 13. DRIFT spectra collected over HZSM-5, Ag/ZSM-5, Ag-Zn/ZSM-5, and Zn/ZSM-5 catalysts upon pyridine adsorption.

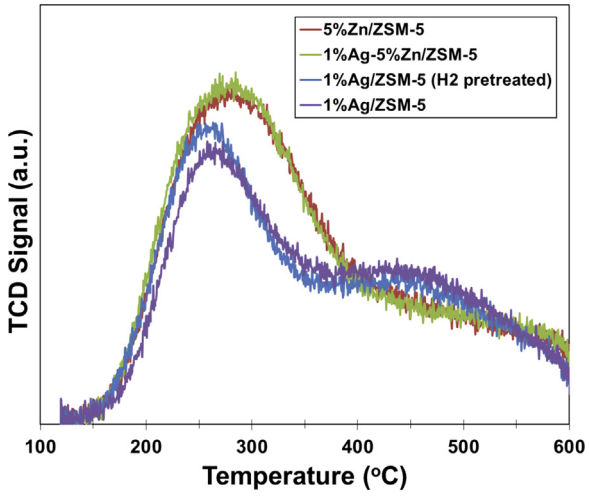

Fig. 14. The NH_3-TPD profiles collected over different catalysts.

Table 7
The average coke formation rate from various ethanol conversion runs performed at 400 °C and 1 atm.

Run	Averaged Coke Formation Rate ($\times 10^{-5}$ mg/mg$_{cat}$ s)
5%Zn/ZSM-5 under methane environment	1.09
1%Ag-5%Zn/ZSM-5 under methane environment	1.12
1%Ag/ZSM-5 under N_2 environment	1.22
1%Ag/ZSM-5 after H_2 pretreatment under N_2 environment	1.23
HZSM-5 under methane environment	1.51
1%Ag/ZSM-5 under methane environment	3.41

ment which also yields significantly less aromatics after referring to Fig. 1. After a second thought, the coke formation might be closely related to the surface acidity of charged catalyst when Figs. 13 and 14 are consulted. Takahara, et al. reported that Brösted acid sites in catalyst are responsible for dehydration of ethanol [6] and the thus formed ethylene is reported as the precursor for coke formation, resulting in catalyst deactivation [28]. More importantly, the carbonaceous residues might be mainly derived from over-aromatization triggered by strong surface acidic sites which are abundant on Ag/ZSM-5 surface as noticed in Fig. 14, leading to the formation of polyalkylaromatics and polyaromatics which are known as coke precursors [42]. Therefore, the surface acidity adjustment of the catalyst would benefit aromatics formation with acceptable coke deposition. Fig. 15c might demonstrate the step we made toward this direction. After hydrogen pretreatment, the Ag/ZSM-5 catalyst exhibits better resistance to coke formation while presenting better aromatization performance as shown in

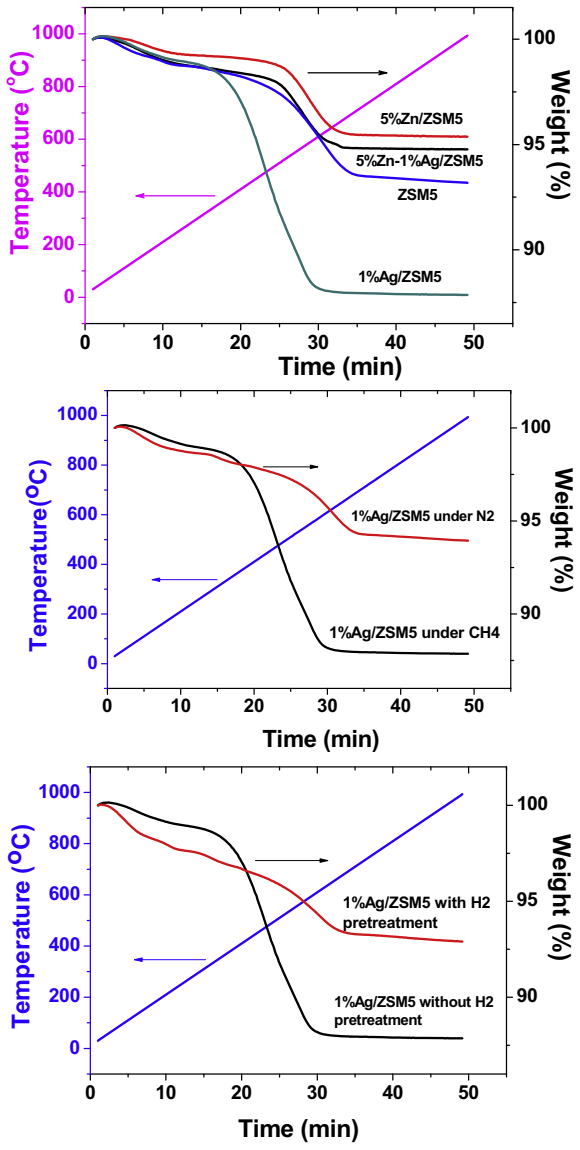

Fig. 15. TGA profiles collected over (a) various spent catalysts and spent Ag/ZSM-5 (b) under different environments, and (c) with or without H_2 pretreatment under heating in air.

Fig. 2. The H_2 pretreatment might not only reduce the Ag to its metallic form, but also change the surface acidity and/or adjust the distribution of Lewis and Brösted acid sites, which deserves further study.

4. Conclusions

The present work demonstrates the technical feasibility of simultaneous aromatization of ethanol and methane over Ag- and Zn-modified zeolite catalyst under mild conditions. Among them, 1%Ag/ZSM-5 demonstrates the most promising catalytic performance in terms of aromatics formation and ethanol conversion at 400 °C and 1 atm under methane environment. The aromatization activity of Ag/ZSM-5 catalyst can be further enhanced through hydrogen pretreatment, which is better than the one collected from the catalytic ethanol conversion under H_2 environment. Methane presence may not only enhance ethanol aromatization, but also get itself activated and being incorporated into the formed aromatics leading to increased carbon number and more endothermic reaction feature. The excellent catalytic performance of Ag/ZSM-5 might be because of the better dispersion of Ag on the ZSM-5 surface and abundant strong Brösted and Lewis surface acid sites which may also result in coke formation. Therefore, tuning the surface acidity of charged catalyst for balancing its aromatization performance and coke resistance for stability enhancement would be a critical future work.

Acknowledgement

We gratefully acknowledge the financial supports from Natural Sciences and Engineering Research Council of Canada (NSERC, RGPIN/04385-2014).

References

[1] BP Statistical Review of World Energy 2015.
[2] Energy Information Administration (EIA).
[3] H. Song, L. Zhang, U. Ozkan, Investigation of the reaction network in ethanol steam reforming over supported cobalt catalysts, Ind. Eng. Chem. Res. 49 (2010) 8984–8989.
[4] K. Van der Borght, V. Galvita, G. Marin, Ethanol to higher hydrocarbons over Ni, Ga, Fe-modified ZSM-5: effect of metal content, Appl. Catal. A: Gen. 492 (2015) 117–126.
[5] N. Viswanadham, S. Saxena, J. Kumar, P. Sreenivasulu, D. Nandan, Catalytic performance of nano crystalline H-ZSM-5 in ethanol to gasoline (ETG) reaction, Fuel 95 (2012) 298–304.
[6] I. Takahara, M. Saito, M. Inaba, K. Murata, Dehydration of ethanol into ethylene over solid acid catalysts, Catal. Lett. 105 (2005) 249–252.
[7] A. Haryanto, S. Fernando, N. Murali, S. Adhikari, Current status of hydrogen production techniques by steam reforming of ethanol: a review, Energy Fuels 19 (2005) 2098–2106.
[8] M. Ni, D. Leung, M. Leung, A review on reforming bio-ethanol for hydrogen production, Int. J. Hydrogen Energy 32 (2007) 3238–3247.
[9] P. Vaidya, A. Rodrigues, Insight into steam reforming of ethanol to produce hydrogen for fuel cells, Chem. Eng. J. 117 (2006) 39–49.
[10] A. Széchényi, R. Barthos, F. Solymosi, Aromatization of ethanol on Mo_2C/ZSM catalysts, Catal. Lett. 110 (2006) 85–89.
[11] R. Barthos, A. Széchényi, F. Solymosi, Decomposition and aromatization of ethanol on ZSM-based catalysts, J. Phys. Chem. B 110 (2006) 21816–21825.
[12] M. Inaba, K. Murata, M. Saito, I. Takahara, Ethanol conversion to aromatic hydrocarbons over several zeolite catalysts, React. Kinet. Catal. Lett. 88 (2006) 135–142.
[13] J. Shu, A. Adnot, B. Grandjean, Bifunctional behavior of Mo/HZSM-5 catalysts in methane aromatization, Ind. Eng. Chem. Res. 38 (1999) 3860–3867.
[14] Y. Xu, L. Lin, Recent advances in methane dehydro-aromatization over transition metal ion-modified zeolite catalysts under non-oxidative conditions, Appl. Catal. A: Gen. 188 (1999) 53–67.
[15] V. Abdelsayed, D. Shehawat, M. Smit, Effect of Fe and Zn promoters on Mo/HZSM-5 catalyst for methane dehydroaromatization, Fuel 139 (2015) 401–410.
[16] P. Tang, Q. Zhu, Z. Wu, D. Ma, Methane activation: the past and future, Energy Environ. Sci. 7 (2014) 2580–2591.
[17] R. Horn, R. Schlögl, Methane activation by heterogeneous catalysis, Catal. Lett. 145 (2015) 23–39.
[18] K. Skutil, M. Taniewski, Some technological aspects of methane aromatization (direct and via oxidative coupling), Fuel Process. Technol. 87 (2006) 511–521.
[19] V.R. Choudhary, A.K. Kinage, T.V. Choudhary, Low-temperature nonoxidative activation of methane over H-galloaluminosilicate (MFI) zeolite, Science 275 (1997) 1286–1288.
[20] O.A. Anunziata, G.V.G. Mercado, L.B. Pierella, Catalytic activation of methane using *n*-pentane as co-reactant over Zn/H-ZSM-11 zeolite, Catal. Lett. 87 (2003) 167–171.
[21] O.A. Anunziata, G.G. Mercado, L.B. Pierella, Improvement of methane activation using *n*-hexane as co-reactant over Zn/HZSM-11 zeolite, Catal. Commun. 5 (2004) 401–405.
[22] M.V. Luzgin, V.A. Rogov, S.S. Arzumanov, A.V. Toktarev, A.G. Stepanov, V.N. Parmon, Methane aromatization on Zn-modified zeolite in the presence of a co-reactant higher alkane: how does it occur? Catal. Today 144 (2009) 265–272.
[23] V.R. Choudhary, K.C. Mondal, S.A.R. Mulla, Simultaneous conversion of methane and methanol into gasoline over bifunctional Ga-, Zn-, In-, and/or Mo-modified ZSM-5 zeolites, Angew. Chem. Int. Ed. 44 (2005) 4381–4385.
[24] P. He, H. Song, Catalytic conversion of biomass by natural gas for oil quality upgrading, Ind. Eng. Chem. Res. 53 (2014) 15862–15870.
[25] P. He, W. Shan, Y. Xiao, H. Song, Performance of Zn/ZSM-5 for in situ catalytic upgrading of pyrolysis bio-oil by methane, Top. Catal. 59 (1) (2016) 86–93.
[26] Y. Xiao, P. He, W. Cheng, J. Liu, W. Shan, H. Song, Converting solid wastes into liquid fuel using a novel methanolysis process, Waste Manage. 49 (2016) 304–310.

[27] A. Guo, C. Wu, P. He, Y. Luan, L. Zhao, W. Shan, H. Song, Low-temperature and low-pressure nonoxidative activation of methane for upgrading heavy oils, Catal. Sci. Technol. 6 (2016) 1201–1213.
[28] H. Song, U.S. Ozkan, Adsorption/desorption behavior of ethanol steam reforming reaction products and intermediates over supported cobalt catalysts, Catal. Lett. 141 (2011) 43–54.
[29] E. Pretsch, P. Buhlmann, M. Martin Badertscher, Structure Determination of Organic Compounds Tables of Spectral Data Fourth, Revised and Enlarged Edition, Springer, 2009.
[30] B. Bachiller-Baeza, J.A. Anderson, FTIR and reaction studies of styrene and toluene over silica–zirconia-supported heteropoly acid catalysts, J. Catal. 212 (2002) 231–239.
[31] S. Almutairi, B. Mezari, E.A. Pidko, P. Magusin, E. Hensen, Influence of steaming on the acidity and the methanol conversion reaction of HZSM-5 zeolite, J. Catal. 307 (2013) 194–203.
[32] D. Yi, H. Huang, X. Meng, L. Shi, Adsorption-desorption behavior and mechanism of dimethyl disulfide in liquid hydrocarbon streams on modified Y zeolites, Appl. Catal. B Environ. 148–149 (2014) 377–386.
[33] W. Xu, S. Miller, P. Agrawal, C. Jones, Zeolite topology effects in the alkylation of phenol with propylene, Appl. Catal. A Gen. 459 (2013) 114–120.
[34] R. Buzzonal, S. Bordiga, G. Ricchiardi, A. Zecchina, Interaction of pyridine with acidic (H-ZSM5, H-β, H-MORD zeolites) and superacidic (H-Nafion membrane) systems: an IR investigation, Langmuir 12 (1996) 930–940.
[35] V.P. Glazunov, S.E. Odinokov, Infrared spectra of pyridinium salts in solution—II. Fermi resonance and structure of NH bands, Spectrochim. Acta 38A (1982) 399–408.
[36] T. Phung, L. Hernández, A. Lagazzo, G. Busca, Dehydration of ethanol over zeolites, silica alumina and alumina: Lewis acidity, Brønsted acidity and confinement effects, Appl. Catal. A: Gen. 493 (2015) 77–89.
[37] W. Liu, Y. Xu, Methane dehydrogenation and aromatization over Mo/HZSM-5: in-situ FT-IR characterization of its acidity and the interaction between Mo species and HZSM-5, J. Catal. 185 (1999) 386–392.
[38] F. Lonyi, J. Valyon, On the interpretation of the NH_3-TPD patterns of H-ZSM-5 and H-mordenite, Microporous Mesoporous Mater. 47 (2001) 293–301.
[39] H.G. Karge, Comparative measurements on acidity of zeolites, Stud. Surf. Sci. Catal. 65 (1991) 133–156.
[40] Y. Shu, Y. Xu, S. Wang, L. Wang, X. Guo, Promotional effect of Ru on the dehydrogenation and aromatization of methane in the absence of oxygen over Mo/HZSM-5 catalysts, J. Catal. 170 (1997) 11–19.
[41] R. Barthos, A. Széchenyi, F. Solymosi, Decomposition and aromatization of ethanol on ZSM-based catalysts, J. Phys. Chem. B 110 (2006) 21816–21825.
[42] P. Dejaifve, A. Auroux, P.C. Gravelle, J.C. Védrine, Methanol conversion on acidic ZSM-5, offretite, and mordenite zeolites: a comparative study of the formation and stability of coke deposits, J. Catal. 70 (1981) 123–136.